ADVANCED FUNCTIONAL MATERIALS
www.afm-journal.de

Bioinspired and Hierarchically Textile-Structured Soft Actuators for Healthcare Wearables

Mengxin Yang, Jing Wu, Wenjie Jiang, Xiaorui Hu, Mohammad Irfan Iqbal, and Fengxin Sun**

Soft pneumatic actuators possess the increasing potential for various healthcare applications, such as smart wearable devices, safe human-robot interaction, and flexible manipulators. However, it is difficult to translate the existing technologies to commercial applications due to their inefficient volumetric power, sophisticated control with high operation pressure, slow production, and high cost. To overcome these issues, herein, a caterpillar-inspired actuator using hierarchical textile architectures based on simple fabrication and low-cost strategy is designed. Unlike the existing textile-based pneumatic actuators, the designed actuators are constructed by combining boucle fancy yarns with a novel trilayer-knit architecture. The as-prepared actuators concurrently possess fast response (1100° s^{-1}), large bending actuation strain (1080° m^{-1}), high-power density (272 W m^{-3}), mechanical robustness, easy-programmable motions, and human-tactile comfort, which outperforms currently reported textile-based pneumatic actuators. Furthermore, due to the geometrical transition of the engineered hierarchical structure, the developed actuators exhibit superior dual-stiffness effect with stress evolution, providing a facile approach to addressing the conflict of flexibility and force output in soft fluidic actuators. This concept as a paradigm provides new insights to develop soft actuators with outstanding design flexibility, adaptability, and multifunctionality using engineered textile-structure, which has great potential for real-world applications in medical rehabilitation, physiotherapy, and soft robotics.

1. Introduction

Soft actuators with high flexibility, excellent compliance, superior power density, and safe interaction are finding unique advances in performing complex tasks, such as internal surgical operations,[1,2] agricultural harvesting,[3] flexible manipulators,[4,5] and wearable devices,[6] that are not possible with conventional linkage rigid robots.[7–14] Recently soft actuators stimulated by pneumatic pressure have attracted wide interest in developing soft actuators and robotics due to their relatively simple and rapid actuation.[15–17] The most common materials used in designing pneumatic soft robotics are silicon-based elastomers, polyethene elastic films, and rubber.[5,18–20] However, the manufacturing of these elastomers generally requires replacing different matched molds to cast the actuators with different structures and morphologies,[21] thereby achieving desired actuation performance and motion styles, which induces costly manufacturing and time-consuming fabrication.[22–24] Despite the high elasticity of these elastomers enhancing the actuation strain and compliance of designed actuators, the relatively low force output and load capacity of such actuators have limited them in practical use for many tasks.[25] 3D printing has been emerging as a convenient approach for fabricating different types of actuators;[26–28] however, the limited processing scale and narrow material adaptability of the printed actuators restrict their versatile applications.[27] Moreover, these actuators are not suitable for next-to-skin wearable interactions due to their poor human-touch comfort.

Textiles are a type of traditional soft materials that can be found in everyday applications in the form of clothing, curtains, beddings, shoes, filters, and face masks have emerged as a promising candidate for designing soft actuators for healthcare wearables,[29,30] due to their flexibility, lightweight, breathability, and comfort tactile-feeling characteristics.[31,32] Recent advances in pneumatic textile-based actuators serve as the foundation of ease-fabrication and low-cost production methods for the actuators.[33–35] A typical mechanism in previous work is to combine conventional fabrics (such as woven and knit) or construct asymmetric layers by folding and pleating fabrics to act as

M. Yang, J. Wu, W. Jiang, F. Sun
Key Laboratory of Eco-textiles of Ministry of Education
Jiangnan University
Wuxi 214122, China
E-mail: fxsun@jiangnan.edu.cn
X. Hu
College of Design
Jiangnan University
Wuxi 214122, China
M. I. Iqbal
Department of Civil Engineering
The University of Hong Kong
Hong Kong S.A.R 999077, China
E-mail: miiqbal@hku.hk
F. Sun
Laboratory of Soft Fibrous Materials
College of Textiles Science and Engineering
Jiangnan University
Wuxi 214122, China
The ORCID identification number(s) for the author(s) of this article can be found under https://doi.org/10.1002/adfm.202210351.

DOI: 10.1002/adfm.202210351

assistive roles (such as anchoring or active roles) for regulating the actuation of the textile actuators.[30,33,36] Despite the inherent anisotropic mechanics of woven and knitted fabrics,[37,38] the existing textile-based actuators still tend to expand in all directions when pressured, resulting in a large volume change even in the unexpected dimension and a low actuation strain (Figure S1, Supporting Information). As a result, a large surrounding space is occupied for operating the actuators, and the actuation efficiency and output forces are thus low. Therefore, instead of combining the conventional structure blocks, developing desirable novel structures for high-performance textile-based actuators will be of great significance to accelerating the development and practical application of soft actuators.

To overcome the above-mentioned drawbacks, the hierarchically designable textile structures, ranging from yarn to fabric levels, provide good potential, but few studies have been carried out regarding unconventional structures for textile actuators to date. Fancy yarns have been widely used for functional textiles because of their controllable structure using industrial wrapping[39] and embedding technologies,[40] and the unconventional shape characteristics enable the fancy yarns with tunable mechanical performance.[41] Moreover, diverse knit architectures with multiple unit loops can be an ideal candidate for modification,[42,43] thereby developing novel composite structures to realize unique properties for the new generation of textile-based actuators. However, neither fancy yarn structures nor modified knit architectures have been considered for developing fabric-based actuators yet.

Herein, for the first time, we report a caterpillar-like pneumatic actuator with a hierarchical structure design from boucle fancy yarn to a trilayer-knit architecture. The hierarchical textile structure enables caterpillar-like actuators with a very high deformation in high-elastic zone but quite low deformation in low-elastic zone, and thus maximally convert the supplied pressure into effective actuation strain and work output, which mimics the caterpillars that consist of many small segments with intermediate elastic skin part and nondeformable exoskeleton part (**Figure 1**a). The elastic skin can bend and stretch to enable caterpillar dexterous crawling, while the exoskeleton acts as protection for entrails during the crawling. Inspired by the caterpillar motion, the proposed actuators with anisotropic deformation achieve outstanding performance on high-power

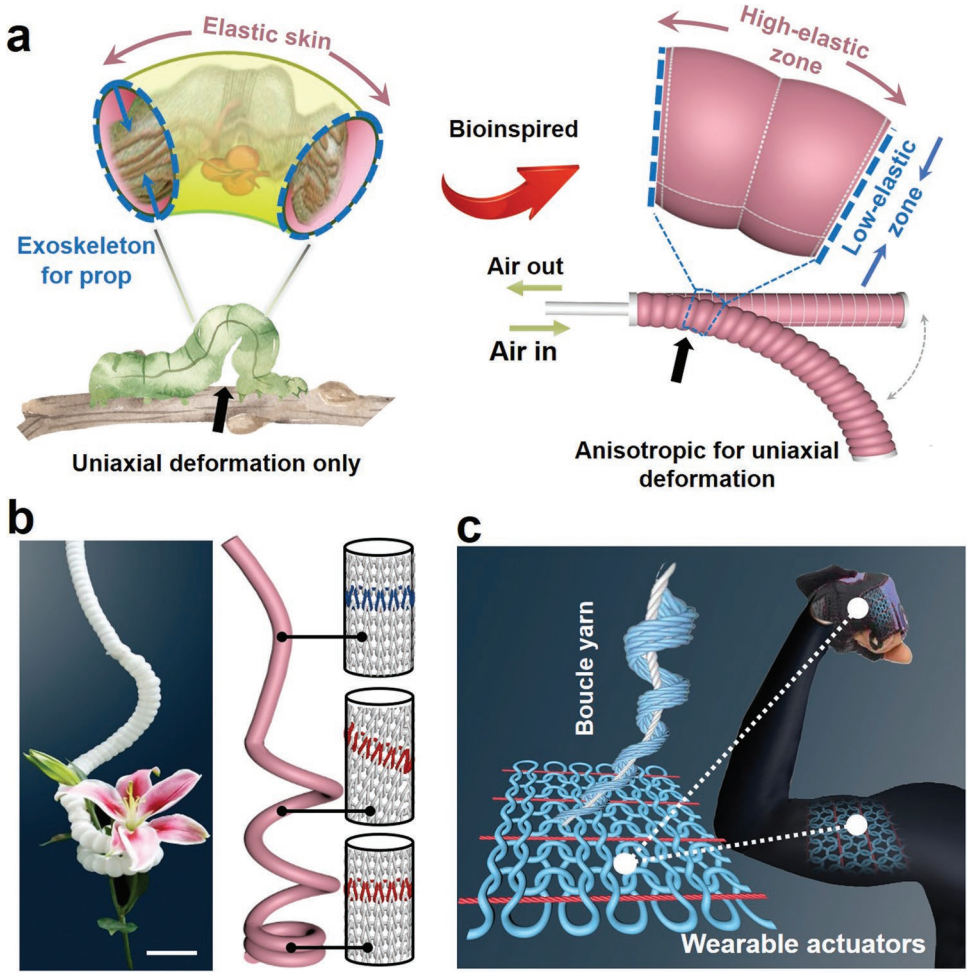

Figure 1. Bioinspired design and functional diversity of the caterpillar-like actuators. a) Anisotropic uniaxial deformation of the actuator for bending actuation inspired by the caterpillars. b) Application of the caterpillar-like actuators to soft gripper with different deformations via altering yarn modulus and knitting directions (scale bar: 5 cm). c) Application to assistive wearables for strengthening the human muscle motions.

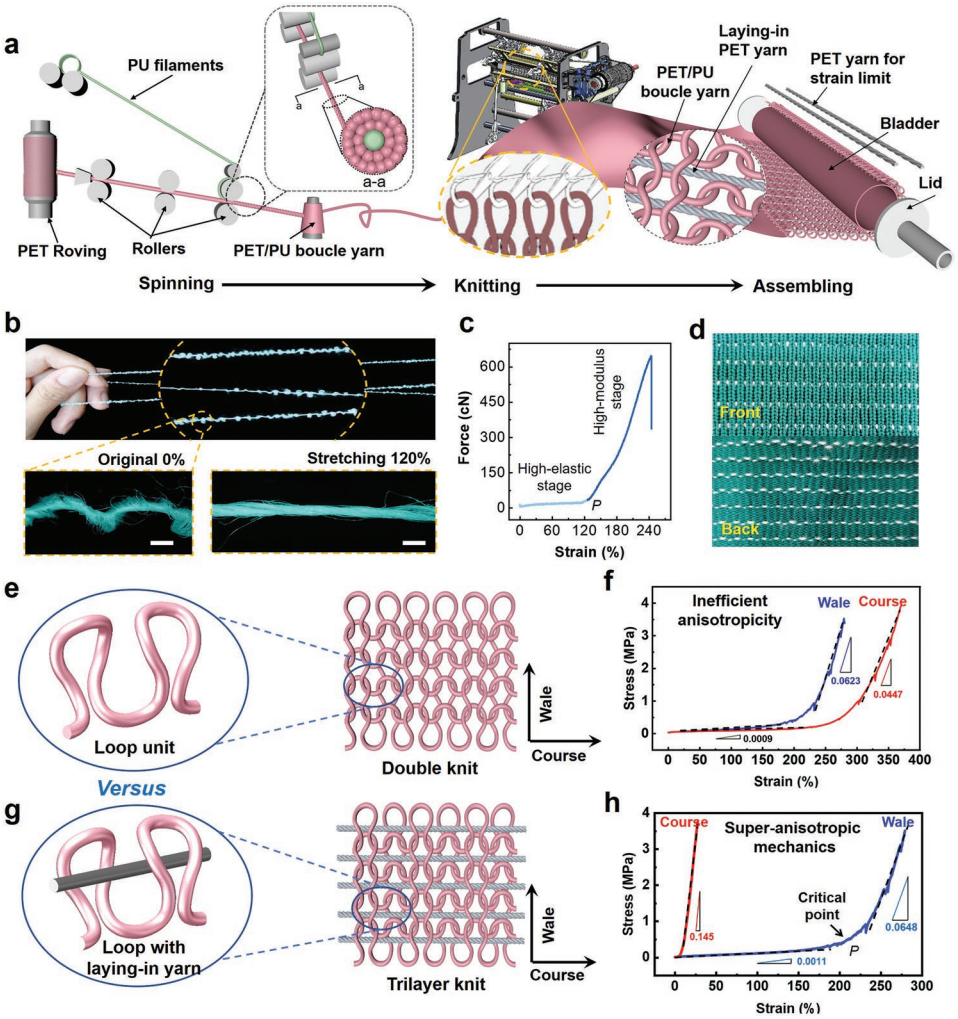

Figure 2. Fabrication and characterization of the hierarchical textile architecture. a) Schematic illustration of the hierarchical fabrication process of the caterpillar-like actuators. b) Photo image of boucle fancy yarns and the optical micrograph images of the yarns under original state and stretched state of 120% elongation (scale bar: 400 µm). c) Mechanical property of the boucle yarn, showing the dual-stiffness tensile property with respect to the critical point $P \approx 120\%$ strain. d) Photo image of the front and back sides of the trilayer-knit architecture. The laying-in yarns (white) are interlocked by the looped boucle yarns (green). e–h) Comparisons between conventional double knit and trilayer knit. e) and g) reveal the property origination by loop unit and topological knit architectures. f) and h) show the typical mechanical properties of double knit and trilayer knit in terms of anisotropicity and dual-stiffness property.

density, fast response speed, large bending actuation strain, and multi-modal deformations, such as bending, spiraling and twisting, for versatile applications without the need for energy-intensive and complex control systems (Figure 1b,c). This research could contribute to the real-world application of new generation of textile-based actuators and expand the healthcare wearable market.

2. Results and Discussion

2.1. Hierarchical Structure Design and Fabrication

To critically address the current limitations and achieve the balanced performance of textile-based actuators in flexibility, actuation force/strain, power density, usability, and controlling complexity, a hierarchical-structured design of textiles is elaborately integrated to fabricate the caterpillar-like actuators. Modern textile technologies enable easy fabrication of the featured hierarchical structures from boucle fancy yarns to complex knitted fabrics (**Figure 2**a; Figure S2, Supporting Information). The boucle fancy yarns are spun based on a sheath-core structure with polyurethane (PU) filaments as core and twisted polyester (PET) fibers as sheath. PU filaments are selected due to its outstanding superelasticity, and PET roving is used to spin the sheath layer because PET is low-cost and the most commonly used synthetic material with relatively high strength and modulus in regular wearables (Figure S3, Supporting Information). During the spinning process, the PET roving is drawn and twisted in a programmed routine, followed by wrapping on the negatively feeding PU filaments, thereby forming a bead-like structure resulting from the contraction of

the PU filaments in a free state (Figure 2b). Remarkably, this fancy structure endows the yarn with a unique dual-stiffness property with a high-elastic stage and a high-modulus state separated by the critical point *P*, where the "beads" on the yarn just disappear along with a snap-through transition from bending deformation to stretching deformation of the PET fibers in the boucle yarn (Figure 2c). Such a remarkable dual-stiffness property plays a vital role in balancing the flexibility and actuation force of soft actuators, providing a simple approach to break boundaries of softness and rigidity in inflatable actuators.

As a basic unit of textiles, the boucle fancy yarns can be naturally used to fabricate 2D fabrics by weaving and knitting techniques. Different from conventional knitted or woven fabrics, we combine the weaving and knitting design principle by looping the boucle yarns to form a double-knit structure and interweaving PET yarns as laying-in yarns to interlock with the knit structure, forming a unified tree-layered composite architecture, which is termed as trilayer knit in this study (Figure 2d; Figure S4, Supporting Information). Such a trilayer knit architecture is quite different from conventional double knitted architectures. As shown in Figure 2e, double knit originates from a loop unit, from which the topological structures generate by continuously interlacing a single yarn. From the view of textile technology, the double knit is fabricated by a single system of yarn, which limits the variation of the mechanical property of the knitted architectures in wale and course directions in terms of yarn properties. As a result, the knitted fabric shows similar large strains in wale and course directions due to the loop deformation and yarn slippage (Figure 2f). Whereas the designed trilayer structure displays a typical two-system-yarn construction with the looped PET/PU yarn and laying-in PET yarn (Figure 2g), endowing the fabric with super-anisotropic mechanical properties. As can be seen from Figure 2h, the trilayer knit shows remarkably higher Young's modulus in course direction than that in wale direction (≈100 times higher when strain <200%). A typical two-stage stretching process can be observed in the whole tensile process of trilayer knit in course direction (Figure S5, Supporting Information). For more intuitive and clearer comparisons with the tensile property of wale direction, we just show the stretching stage of course direction before the breaking of PET yarns occurs in Figure 2h. More interestingly, the trilayer knit also shows a dual-stiffness feature in wale direction and its modulus can be approximately represented by two linear segments, that is, a low modulus (0.0011 MPa) in low strain state (<200%) and an over 50-fold higher modulus (0.0648 MPa) in large strain state (>200%). This can be ascribed to the combined effects of the sequence deformations of the local displacement of stitches and dual-stiffness yarn in a topological knitted structure.[37] The low modulus at the initial stage is linked to the stitch extensions of the fabric and the high-elastic elongation of the boucle yarns enabled by the applied forces and moment (Figures S6 and S7, Supporting Information). Once the PU core is completely compliant with the PET sheath of the boucle yarn and each stitch is drawn up to the maximum geometry deformation, the strain will be restricted by the twisted PET sheath part of the yarn, resulting in the high modulus upon stretching, which can also be verified by the stress nephogram of the finite element analysis, as shown in Figure S8 (Supporting Information). Therefore, the super-anisotropicity and dual-stiffness property of the designed trilayer knitted architecture is considered to provide good potential for critically addressing the problems in balancing the actuation strain, actuation force, power density, and deformation speed of existing soft actuators, which will be further discussed in the following section.

2.2. Actuation Performance of the Textile Actuators

The trilayer-knit fabric can be integrated with inside bladders to assemble a caterpillar-like trilayer-knit actuator (details in Experimental Section). During the fabrication process, a PET yarn is used to sew the 2D fabric into designed shape, such as 3D tube. The PET yarn is thereby leveraged as the strain-limiting yarn to achieve bending actuation. The trilayer-knit actuator can generate large bending strain (over 216°) with an ultrafast speed (up to 1100° s^{-1}) when operated by air pressure of 50 kPa (**Figure 3**a; Figure S9, Supporting Information), which outperforms most of currently reported textile-based actuators (Table S1, Supporting Information). The power density ($P_D = P/V$) of 272 W m^{-3} is estimated by the actuation power ($P = m_{\text{actuator}} G\Delta h/t = 0.0109$ W) and actuator volume of 4.02×10^{-5} m^3), where $m_{\text{actuator}} = 8$ g is the mass of actuator, G is gravitational acceleration, $\Delta h = 6.7 \times 10^{-2}$m is vertical displacement of actuator's barycenter, and $t = 0.49$ s is the actuation time (Figure 3a). Such a high-power density is comparable to human skeletal muscles (50–248 W m^{-3}).[17]

In contrast, the conventional double-knit-based actuator shows significantly smaller bending strain and a longer period of actuation time, but larger expansion in radial direction, thereby displaying low-energy transmission (Figure 3b; Movie S1, Supporting Information), while the novel trilayer-knit actuator is free of these problems. This is because the novel two-system-yarn architectures where the laying-in PET yarns in the trilayer knit restrict the radial deformation of actuators, and enhance the longitudinal deformation due to the unidirectional slippage of loop yarns. Whereas the slippage of loop yarns deteriorates in the double-knit-based actuators as the fabric tends to be biaxially stretched upon inflation, and self-locking happens at the interlacing points of stitches considering the aforementioned single system of yarns, thus sacrificing the inherent elasticity of double-knit architectures instead.

The quantitative comparisons are shown in Figure 3c,d. Impressively, the trilayer-knit actuator shows an obvious increase in the output force when the supplied pressure is over 40 kPa, which corresponds to the aforementioned dual-stiffness features of the trilayer knit, and the actuator can exert a high force up to 120 cN on its tip under a supplied pressure of 70 kPa (Figure 3c). This force is over ten times of the gravity from its own weight (8 g). Meanwhile, the bending actuator can rapidly bend to over 120° in 0.31 s under a low pressure of 50 kPa (Figure S9, Supporting Information) when the strain of the trilayer knit remains lower than the critical strain, which critically addresses the problems in balancing the flexibility (easy deformation) and actuation force (high force output). As shown in Figure 3d, the double-knit-based actuator displays small bending deformation with maximum curvature <0.05 cm^{-1} even the supplied pressure increasing to 60 kPa,

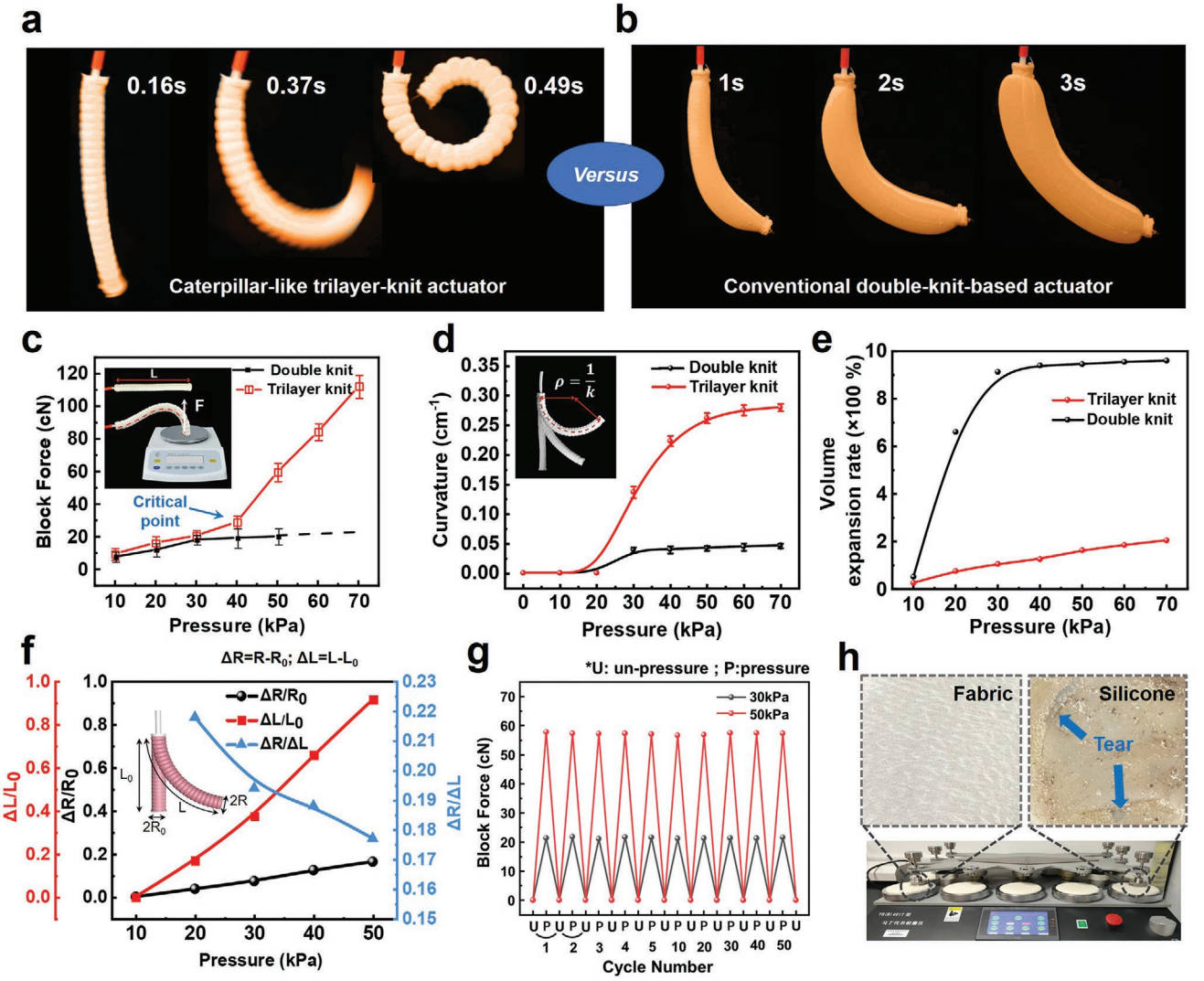

Figure 3. Actuation performance of the caterpillar-like actuators. a) Photo images displaying the fast-speed and large bending actuation strain of caterpillar-like trilayer-knit actuator within 0.49 s under supplied pressure of 50 kPa. b) Photo images showing the bending actuation of conventional double-knit actuator within 3 s under supplied pressure of 50 kPa. c) Blocking force under different applied pressures (original dimensions of the actuator: 20 cm in length and 1.6 cm in diameter). d) Bending curvatures of the actuators fabricated by double knit and trilayer knit. e) Volume expansion ratio under different applied pressures. f) Changing ratio of geometrical dimensions of the caterpillar-like bending actuators upon inflation. g) Reversible cyclic changes of the blocking force over 50 cycles of the caterpillar-like actuator at different pressures (30 and 50 kPa). h) Wearability test by a Martindale abrasion tester, showing the robust mechanical property of the knit fabric compared with silicone elastomer that is generally used for pneumatic actuators.

but a large volume expansion ratio (Figure 3e), resulting not only in a waste of operating space but also in energy dissipation for efficient actuation. On contrary, a small volume expansion and large actuation deformation can be observed in the designed actuator made with trilayer knit, as indicated by much higher bending curvature (>0.25 cm^{-1}) under the same supplied pressure compared with the double-knit actuator. This can be further validated by the relatively low rate of dimension changes ($\Delta R/R_0$<0.2) of the trilayer-knit actuator in radial direction, but large rate of deformation ($\Delta L/L_0$ up to 1.0) in axial direction by augmenting the applied pressure from 0 to 50 kPa (Figure 3f). It should be pointed out that the bending curvature of the bending actuator is mainly determined by the difference of Young's modulus from the outside to inside of the bending beam. With the increase of the supplied pressure, the strain of the outside increases, resulting in higher Young's modulus (Figure 2h) and thereby inducing a smaller difference of Young's modulus between the outside and inside of the bending beam. When the outside Young's modulus approaches to inside Young's modulus, the changes of bending curvature will meet the limited response. Therefore, the bending curvature of the trilayer-knit-based actuator shows a sharp increase with the increase of the supplied pressures from 20 to 40 kPa; whereas, the curvature shows small changes when the pressure is over 50 kPa and nearly becomes constant when the pressure changes from 60 to 70 kPa

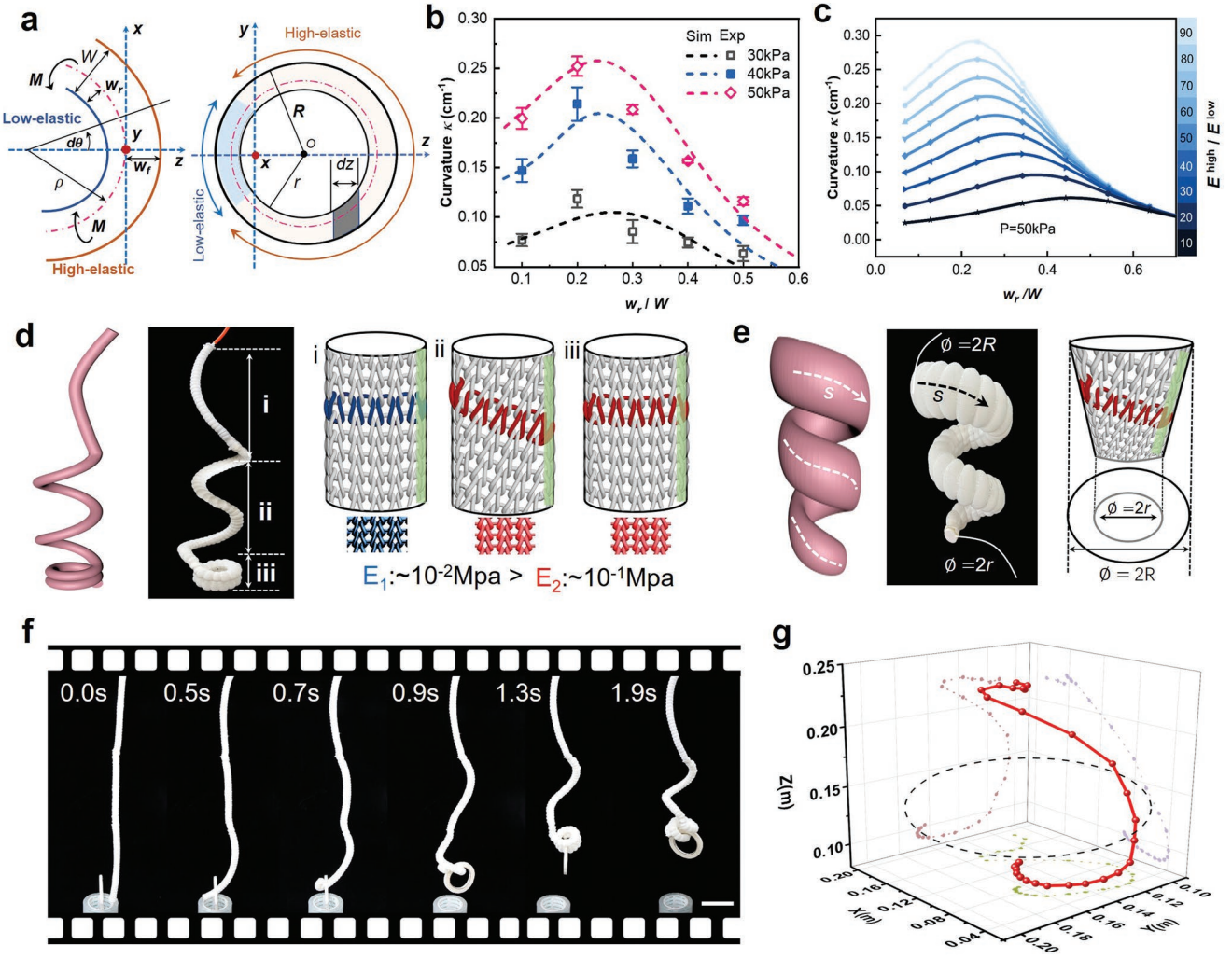

Figure 4. Programming actuators with multi-mode actuation. a) Schematic illustration of the bi-modulus problem based on parameter analysis of longitudinal section and cross section of a bending actuator. b) Theoretical curve and experimental data for bending curvature evolution under different elastic ratios (w_r/W means the ratio of the width of low-elastic region with respect to the whole width). c) Predicted bending curvature as a function of elastic ratios w_r/W at different modulus ratio E^{high}/E^{low} (ratio of the modulus between low-elastic region and high-elastic region). d) Programmed geometry and elastic for multi-mode actuation. Images i–iii show the origin of diverse deformations of the actuator by different yarn moduli and stitch directions. e) Conical helical deformation caused by diameter gradient. f) Images from Movie S2 (Supporting Information) showing the gripping process by sequence rolling and spiraling to lift a tape (scale bar: 10 cm). g) Parallel multi-mode motion of the actuator with unit vector trajectory in a spatial coordinate (pressure range: 0–50 kPa).

(Figure 3d). Moreover, the good repeatability and durability of the trilayer-knit actuator are proved by the stable actuation force tested over 50 actuation cycles (Figure 3g) and wearability test (Figure 3h; Figure S10, Supporting Information), which indicates robust performance of the actuator and can be readily used for practical applications.

2.3. Mechanisms and Inverse Design of Multi-Mode Actuation

A theoretical analysis is further developed to analyze the bending actuation mechanism and structure optimization of the designed actuators via a bi-moduli model. The geometric parameters of the bending actuator, i.e., curvature radius ρ, infinitesimal central angle dθ, width of low-elastic region w_r, width of high-elastic region w_f, and the diameter W, are illustrated in **Figure 4**a. We here treat the low-elastic region and high-elastic region as transverse-isotropic materials, respectively (Text S1, Supporting Information). The actuator possesses a strain gradient in radial direction to render a bending deformation due to the different modulus, so that the axial stresses in the high-elastic and low-elastic regions are estimated by the Equation 1 and Equation 2,

$$\sigma_x|_{z\geq 0} = \sigma_x^{high} = \frac{E_x^{high}}{1-\nu^2}\left(\frac{z^+}{\rho} + \nu\varepsilon_r\right) \quad (1)$$

$$\sigma_x|_{z<0} = \sigma_x^{low} = \frac{E_x^{low}}{1-\nu^2}\left(\frac{z^-}{\rho} + \nu\varepsilon_r\right) \quad (2)$$

where σ_x is the axial stress of the actuator, E_x^{high} and E_x^{low} are the Young's modulus of high-elastic and low-elastic regions, respectively, v is the Poisson's ration. Considering the force and moment equilibrium relationships, we derived the following relations,

$$\frac{2}{M}\frac{1+v^2}{1-v^2}\left(H(w_f)E_x^{high}+K(w_r)E_x^{low}\right)=\rho \quad (3)$$

Here $H(w_f)=\frac{t}{3}w_f^3+\frac{t}{5R(R-t)}w_f^5$, $K(w_r)=\frac{t}{3}w_r^3+\frac{t}{5R(R-t)}w_r^5$, and $t = R\text{-}r$. It can be deduced from the Equation 3 that the curvature radius ρ and curvature $\kappa = 1/\rho$ are mainly determined by the designed geometry parameters, (i.e., R, t, w_f, w_r), and Young's modulus of high-elastic region E_x^{high} and low-elastic region E_x^{low} (Details in Supporting Information). To further investigate the effect of the geometry parameters on the mechanical property to optimize the actuation performance of the actuator, the relationship between curvature κ and the width ratio w_r/W, (where $W = w_r+w_f$) is simulated by detailed calculation and compared with the experimental results under pressures of 30, 40, and 50 kPa (Text S2, Figures S11 and S12, Supporting Information). A good agreement is observed between the simulation and experiment, and the maximum values of the curvature are obtained when the ratio w_r/W ranges from 0.2 to 0.3 (Figure 4b). This result suggests that proper selection of the width ratio of low-elastic region to the whole region within 0.2–0.3 is very important to achieve large bending curvature for the actuators. Moreover, the effect of the modulus ratio (E^{high}/E^{low}) and actuator radius on the bending curvature of the actuator are simulated (Figure 4c; Figure S13, Supporting Information). As expected, the bending curvature increases with the increase of the modulus ratio, while it decreases with the increase of the radius, providing a guidance for optimizing bending actuation strain in practical usage.

Based on the experimental results and theoretical analysis, the as-prepared trilayer-knit actuators can be easily programmed to perform different deformations, including bending, spiraling, and rolling, by simply regulating the fiber/yarn modulus, knitting stitches, and trimming angles of the fabrics (Figure 4d,e). The fabric with high modulus in elastic regions results in a low modulus ratio according to the simulation in Figure 4c, while low modulus in elastic regions can induce large bending curvature of the actuator upon inflation. Interestingly, by arranging knitting stitches in an angle of ≈45°, we can easily create a tendril-like spiraling actuator (Figure 4d) without requiring any complex casting and post-processing. As a result, various actuators with different configurations are assembled to form multi-mode actuation strains when driven by a single air source for a variety of desirable motions. In addition, the bending curvature of the actuator can be further programmed by tuning the radius to realize tentacle-like movements according to Equation 3 and simulation results in Figure S13 (Supporting Information). A conical actuator is fabricated by adjusting its radius size to achieve different bending effects (Figure 4e), with a wide range of curvature changes from 0.14 to 0.23 cm^{-1} upon inflation under different pressures (30, 40, and 50 kPa) (Figure S14, Supporting Information).

Such a versatile actuator can be used as a soft gripper, and a sequential deformation is achieved by reasonably programming the modulus of the fabric and regulating knitting stitches without the need of complex control systems (Figure 4f). The curling part (section iii of Figure 4d) of the actuator can scoop up objects, showing a large contact area with gripped objects, thereby providing a more effective grasping capability, especially for objects with irregular shapes. The spiral part (section ii of Figure 4d) displays more complex kinematic morphology than simple curling deformation to achieve a high contraction stroke to lift the gripped objects following the gripping process. The bending contraction and extension portions deform in an orthogonal direction to enable transformation in different planes and to enlarge the working space (Figure 4g; Figure S15, Supporting Information). Furthermore, the actuator is very pliable and thus can adapt to the shape, weight, and configuration of objects without damaging fragile objects. Versatile applications of the fabric-based actuator to gripping and lifting different objects such as flowers, bananas, and vases with a weight range from 30 to 300 g are demonstrated in Figure S16 (Supporting Information). The actuator of ≈19 g can lift a 300 g vase that is ≈16 times higher than its own weight. A real-time feedback of the grip force by mimicking human touch feeling is also measured by a flexible pressure sensor (FlexiForce) on the surface of the actuator (Figure S16, Supporting Information), which shows a stable gripping force under each supplied pressure. The gripping force is closely associated with the curvature change of the bending actuator, and the curvature change is further determined by the supplied pressure. Since the change of the curvature becomes small when the pressure is over 40 kPa (Figure 3d), the gripping force shows a small increase and tends to be stable with the pressure increasing from 40 to 70 kPa (Figure S16, Supporting Information). The real-time measurement and analysis of the gripping force deserves further studies by integrating textile-based stress sensors into the actuators to design self-sensing and smart textile-based actuators.

2.4. Applications for Healthcare Assistive Devices

Unlike rigid exoskeletons that currently exist for assistive medical rehabilitation, high-performance textile-based actuators can provide good wearing comfort with inherent breathability, flexibility and good tactile feelings (Figure S17, Supporting Information), and thus the application of trilayer-knit actuators for wearable robots greatly enhances the safety of human-machine interaction.[44,45] **Figure 5**a shows a wearable actuator fabricated using a trilayer knit to assist arm motions. The actuator with a length of 20 cm is worn on a fake arm, producing a bending moment over 0.25N m, while lifting a mass of 225 g with respect to the elbow (Figure 5a,b) with only a supplied pressure of 40 kPa. The pressure-moment curve displays a good linear relationship when the air pressure ranges from 10 to 40 kPa, providing a convenient way to regulate and control the actuators in real-world applications. Moreover, the trilayer-knit actuators are also integrated into a glove to assist fingers with flexion and extension motions (Figure 5c). The textile-based pneumatic glove shows good foldability and conformability, and is

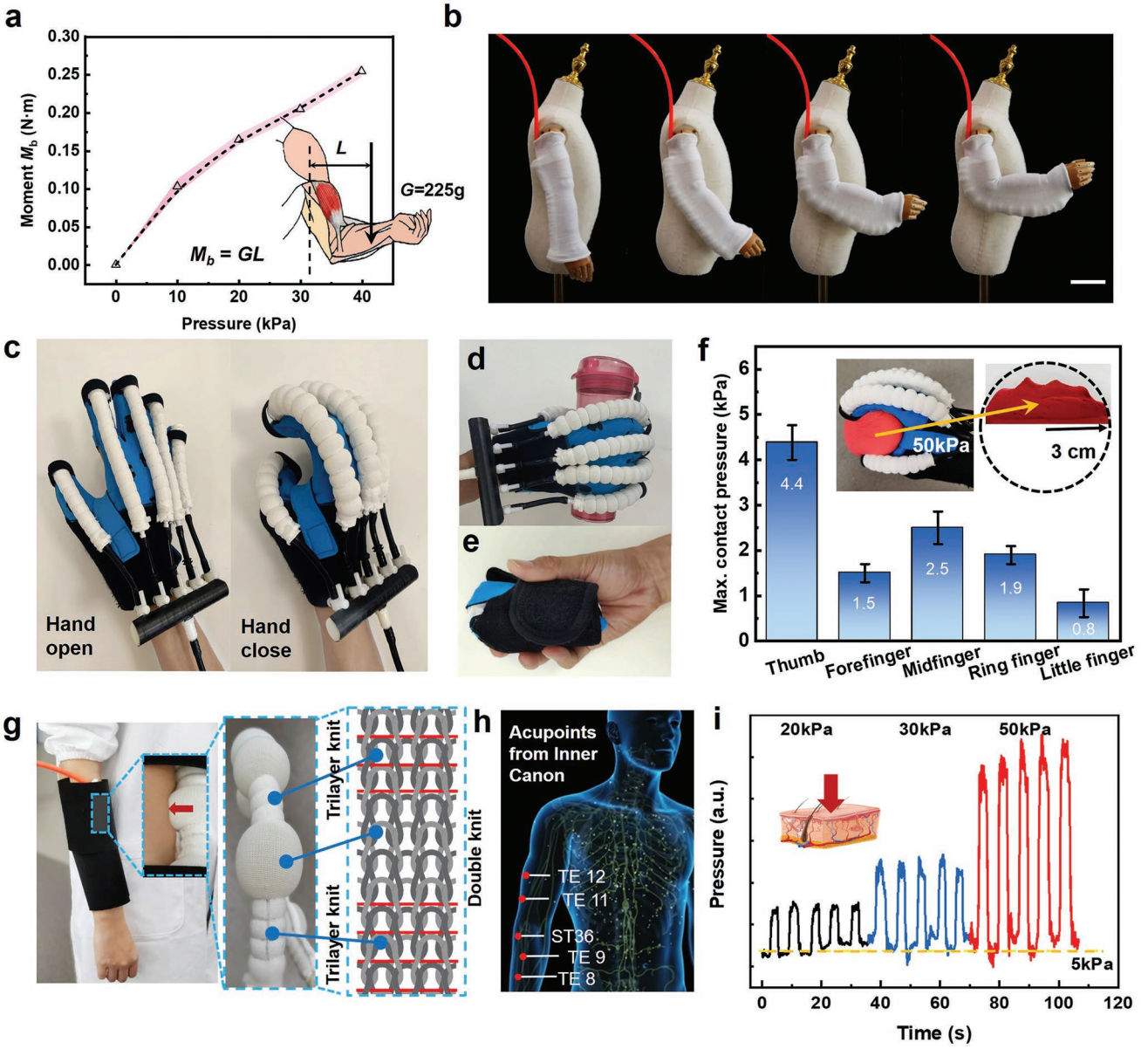

Figure 5. Applications of the trilayer-knit actuators for healthcare assistive wearables. a) Exerting moment M_b of the actuator on a 225 g fake arm as a function of supplied pressure. b) Sequence images showing a concept usage of the actuator for wearable mobility aids (scale bar: 10 cm). c) Pneumatic glove driven by the trilayer-knit actuators for assisting finger motions. d) Grasping a water bottle with the aid of the pneumatic glove. e) Foldability of the textile-based pneumatic glove. f) The maximum contact pressure of each finger when grasping a cylinder with diameter of 6 cm under a supplied pressure of 50 kPa. g,h) Massage robotic realized by the gourd-like textile actuator via a combination design of trilayer-knit and double-knit structures for pressuring acupuncture points on human arm from Chinese medicine. i) Easy-regulatable pressure output of the massage robotic on the acupuncture points under different supplied pressure.

promising for helping people with hand limitations to grasp objects upon pressurization (Figure 5d,e). To quantitatively analyze the grasping capacity of the pneumatic glove, the grasp pressure of the glove is estimated by grasping a plastic soft material (such as plasticine). Briefly, a healthy participant who wears the glove first move the hand toward a plasticine cylinder with compression modulus of ≈17.5 kPa (Figure S18, Supporting Information), and then a pressure of 50 kPa is supplied to the glove to perform the gripping motion around the cylinder while the participant's hand remains as passive as possible. The peak grasp pressure for each finger can be estimated from the maximum strain of the deformed plasticine, as shown in Figure 5f. The grasp pressure of the thumb is up to 4.3 kPa, and a contact force ≈3N can be estimated by the contact area of thumb pulp with the maximum deformation (≈7 cm^2). This force is sufficient to grasp objects up to a weight of 153 g under a supplied pressure of 50 kPa for the glove when the coefficient of static friction is set to 0.5. In addition, the textile-based pneumatic actuator can be conveniently designed as massage robotics by leveraging a combination of double knit

and proposed trilayer knit by sewing the two pieces of fabrics on both sides of the actuator's axial direction using PET yarns (Figure S19, Supporting Information). The different deformation features of the double knit and trilayer knit result in a concavo–convex morphology of the actuator to form acupuncture points upon inflation (Figure 5g), forming an array to imitate the physical therapist for acupressure (Figure 5h). Furthermore, it also shows great potential for developing standard massaging devices because the massage intensity can be regulated and tuned by simply changing the supplied pressures (Figure 5i), suitable for personal healthcare.

3. Conclusion

Inspired by the motion behavior and anatomy of caterpillar, customizable and reconfigurable textile-based soft actuators with superior actuation performance, mechanical robustness, easy-programmable motions, and human-tactile comfort are designed and demonstrated. Theoretical modeling and simulation confirm the important role of the hierarchical textile design and anisotropic mechanics of trilayer-knit architectures, which allows us to rapidly program, fabricate and realize various actuators, thereby coupling the actuators with multiple motion styles to produce adaptive soft robotics, such as grippers. A great value of the high-performance trilayer-knit actuators for portable healthcare wearables with safer, more comfortable, and practical features is demonstrated. Our concept presented here can also be applicable to other multifunctional wearables that need variable stiffness and anisotropic mechanical behavior.

4. Experimental Section

Materials: PU filament (diameter = ≈145 µm; 40 denier) used for the core materials of the boucle fancy yarns in this study was purchased from Zhuji Likun Chemical Fibre Co Ltd, China. PET roving of 364 tex was used for the fabrication of the twisted sheath materials of the boucle yarns and for the manufacturing of strain-limiting yarns, respectively. Silicone film with thickness of 0.3 mm and shore hardness of 25 was used as inner bladders to prevent air leakage.

Spinning of the Boucle Yarn and PET Yarn: The boucle fancy yarns with the core of PU filament and the sheath of twisted PET fibers were spun using a ring-spinning machine (HJ-JN001, Wuxi Hengjiu Electric Technology Co. Ltd, China). Briefly, the PET roving of 364 tex was fed into the back roller and PU filament of 40 denier was fed from front roller of the ring-spinning machine to produce 15 tex sheath-core boucle yarn with a twist factor α_{tex} = 340 at inserted Z-twisted twists of 870 per m. The total draft ratio is set to 25, where the back daft ratio is 1.2. The PU filament is fed under an applied tension which induces a draft ratio of ≈3.5. The spindle speed is set to 8000 rpm, and roller diameter of 25 mm × 25 mm × 25 mm and roller gauge of 18 mm × 38 mm were used. The relative humidity is kept above 65 ± 2% during the yarn spinning process. Similarly, the PET roving was fed into draft zone of the ring-spinning machine under a total draft of 24 to produce 15 text single-helical PET yarn, followed by the doubling process, and applying S-twist using a two-for-one twister to produce double-helical PET yarn.

Fabrication of the Trilayer Knit: The trilayer knit was fabricated on a two-needle-bar knitting machine (KSC-132, Jinlong Technology Co. Ltd, China) with a gauge of 16 and knit width of 132 cm (52 inch). The boucle yarns and PET yarns were used as loop yarn and laying-in yarn, respectively. The boucle yarns were hooked by the front and back knitting needle at intervals to interlace with each other to alternatively form the front and back loops, and the PET yarn was embedded between loop pairs with the needle position of 0.00P. Due to the contraction of boucle yarn, the actual wale density is measured as 70 per 5 cm, a little higher than the theoretical value. The interval stitches of the trilayer knit can be optimized to enhance the stability in course and maintain the elasticity in wale.

Fabrication of the Actuator: The shell of the actuator was produced by cutting the trilayer knit into 50 mm × 200 mm rectangle shape and sewing the sample into a 3D tube using the self-spun PET yarns. The flat seam was selected for sewing the tube because the stitches have low deformation along the sewn direction, and thus sewn-in PET yarn is leveraged as the strain limiting yarn to achieve bending actuation of fabricated actuator. Then a silicone bladder with diameter of 16 mm and length of 200 mm was inserted into the tube. The lids of plastic polylactic acid (PLA) for sealing the both ends of the bladder were manufactured using a 3D printer (Allcct-Mars2). The basic dimension of the lids is illustrated in Figure S20 (Supporting Information). The lids are glued to the bladder at the edge of the end and further tied with the knit tube by cable ties to avoid any possible air leakage.

Characterization: An electronic universal tester (AGS-X, Shimadzu, Japan) was used to test the tensile properties of yarn with a gauge of 100 mm and testing speed of 250 mm min^{-1}. A Meters CMT6103 tester (MET, USA) was used to measure the tensile properties of the knitted fabrics. In the tensile measurements, samples were clamped at a distance of 100 mm and stretched at a test speed of 100 mm min^{-1}. The morphological structure of the knitted fabric was observed using an optical digital microscope (VHX5000, KEYENCE, Co., Ltd, Osaka, Japan). The blocking force of the actuator was measured by an electronic balance (FA2004N). The trajectory of the actuator tip in the X, Y, and Z directions was captured by a set of digital cameras and drawn with the aid of Tracker software (Avanquest USA LLC). KEITHLEY DMM6500 was used to measure the pressure exerted by the actuator on the object. A high-speed camera (Micro LAB-110, Ametek, USA) was used to capture the movement of the actuator after pressurization. In order to quantify the actuation performance of actuators, the bending actuation strain (*Bas*), and power density (P_D) were defined as:

$$Bas = \frac{\theta_{max,two\text{-}end}}{L_{actuator}} \tag{4}$$

$$P_D = \frac{m_{actuator} G \Delta h}{tV} \tag{5}$$

where $\theta_{max,two-end}$ is the maximum bending angle measured from the tangent line of the two ends of the actuator, $L_{actuator}$ is the length of the actuator, $m_{actuator}$ is the mass of the actuator, G is gravitational acceleration, Δh is vertical displacement of actuator barycenter, V is the inflated volume of actuators, and t is the actuation time.

In wearable study, informed consent forms were signed by participants and no formal approval from institutional authorities was required.

Statistical Analysis: The quantitative data with error bar are represented by mean ± S.D. based on at least three replicates unless stated otherwise. Statistical analysis was conducted on Origin 2018 or Microsoft Excel 2019.

Supporting Information

Supporting Information is available from the Wiley Online Library or from the author.

Acknowledgements

The authors thank Dr. M. Guo and Dr. C. Chen (MOE Engineering Center for Knitting Technology) for their assistance in the fabrication

process. This research was supported by the National Natural Science Foundation of China (NSFC, grant no. 12272149; 11802104), the National Key Research and Development Program (grant no. 2017YFB0309200), and Social Science Foundation of Jiangsu Province (grant no. 20YSC002).

Conflict of Interest

The authors declare no conflict of interest.

Data Availability Statement

The data that support the findings of this study are available in the supplementary material of this article.

Keywords

actuators, bioinspired, healthcare, multi-modal deformations, wearables

Received: September 5, 2022
Revised: October 24, 2022
Published online:

[1] L. Xu, H. Wu, W. Qian, Y. Wang, C. R. Bowen, Z. L. Wang, Y. Yang, *Mater. Today* **2022**, *56*, 42.
[2] I. De Falco, M. Cianchetti, A. Menciassi, *Bioinspir. Biomim.* **2017**, *12*, 056008.
[3] C. Tawk, M. I. H. Panhuis, G. M. Spinks, G. Alici, *Soft Robot.* **2018**, *5*, 685.
[4] K. C. Galloway, K. P. Becker, B. Phillips, J. Kirby, S. Licht, D. Tchernov, R. J. Wood, D. F. Gruber, *Soft Robot.* **2016**, *3*, 23.
[5] B. Mosadegh, P. Polygerinos, C. Keplinger, S. Wennstedt, R. F. Shepherd, U. Gupta, J. Shim, K. Bertoldi, C. J. Walsh, G. M. Whitesides, *Adv. Funct. Mater.* **2014**, *24*, 2163.
[6] L. Cappello, K. C. Galloway, S. Sanan, D. A. Wagner, R. Granberry, S. Engelhardt, F. L. Haufe, J. D. Peisner, C. J. Walsh, *Soft Robot.* **2018**, *5*, 662.
[7] D. Sui, Y. Zhu, S. Zhao, T. Wang, S. K. Agrawal, H. Zhang, J. Zhao, *Soft Robot.* **2022**, *9*, 36.
[8] J. Wang, D. Gao, P. S. Lee, *Adv. Mater.* **2021**, *33*, 2003088.
[9] N. R. Sinatra, C. B. Teeple, D. M. Vogt, K. K. Parker, D. F. Gruber, R. J. Wood, *Sci. Robot.* **2019**, *4*, aax5425.
[10] B. B. Kang, H. Choi, H. Lee, K.-J. Cho, *Soft Robot.* **2019**, *6*, 214.
[11] C. Jiang, D. Wang, B. Zhao, Z. Liao, G. Gu, *Appl. Phys. Rev.* **2021**, *8*, 041416.
[12] B. Gorissen, D. Reynaerts, S. Konishi, K. Yoshida, J.-W. Kim, M. De Volder, *Adv. Mater.* **2017**, *29*, 1604977.
[13] Y. Peng, F. Sun, C. Xiao, M. I. Iqbal, Z. Sun, M. Guo, W. Gao, X. Hu, *ACS Appl. Mater. Interfaces* **2021**, *13*, 54386.
[14] Q. Guan, J. Sun, Y. Liu, N. M. Wereley, J. Leng, *Soft Robot.* **2020**, *7*, 597.
[15] Y. Hao, Z. Gong, Z. Xie, S. Guan, X. Yang, T. Wang, L. Wen, *J. Bionic. Eng.* **2018**, *15*, 220.
[16] Z. Wang, S. Hirai, *IEEE Rob. Autom. Lett.* **2017**, *2*, 624.
[17] M. Li, A. Pal, A. Aghakhani, A. Pena-Francesch, M. Sitti, *Nat. Rev. Mater.* **2022**, *7*, 235.
[18] K. H. L. Heung, R. K. Y. Tong, A. T. H. Lau, Z. Li, *Soft Robot.* **2019**, *6*, 289.
[19] J. D. Greer, T. K. Morimoto, A. M. Okamura, E. W. Hawkes, *Soft Robot.* **2019**, *6*, 95.
[20] T. J. Jones, E. Jambon-Puillet, J. Marthelot, P. T. Brun, *Nature* **2021**, *599*, 229.
[21] Y. Guo, L. Liu, Y. Liu, J. Leng, *Adv. Intell. Syst.* **2021**, *3*, 2000282.
[22] W. Hu, G. Alici, *Soft Robot.* **2020**, *7*, 267.
[23] W. Xiao, D. Hu, W. Chen, G. Yang, X. Han, *J. Bionic. Eng.* **2021**, *18*, 1358.
[24] S. Y. Kim, R. Baines, J. Booth, N. Vasios, K. Bertoldi, R. Kramer-Bottiglio, *Nat. Commun.* **2019**, *10*, 3464.
[25] M. A. Robertson, H. Sadeghi, J. M. Florez, J. Paik, *Soft Robot.* **2017**, *4*, 23.
[26] A. Zolfagharian, A. Z. Kouzani, S. Y. Khoo, A. A. A. Moghadam, I. Gibson, A. Kaynak, *Sens. Actuators, A* **2016**, *250*, 258.
[27] T. J. Wallin, J. Pikul, R. F. Shepherd, *Nat. Rev. Mater.* **2018**, *3*, 84.
[28] M. Schaffner, J. A. Faber, L. Pianegonda, P. A. Ruhs, F. Coulter, A. R. Studart, *Nat. Commun.* **2018**, *9*, 878.
[29] C. Laschi, M. Cianchetti, *Front. Bioeng. Biotechnol.* **2014**, *2*, 3.
[30] V. Sanchez, C. J. Walsh, R. J. Wood, *Adv. Funct. Mater.* **2020**, *31*, 2008276.
[31] Y. Wang, X. Liu, C. Zhu, A. Parsons, J. Liu, S. Huang, I. Ahmed, C. Rudd, N. Sharmin, *J. Mech. Behav. Biomed. Mater.* **2019**, *99*, 47.
[32] L. Liu, L. Wei, F. Sun, *Text. Res. J.* **2021**, *91*, 2872.
[33] L. Cappello, K. C. Galloway, S. Sanan, D. A. Wagner, R. Granberry, S. Engelhardt, F. L. Haufe, J. D. Peisner, C. J. Walsh, *Soft Rob.* **2018**, *5*, 662.
[34] L. Ge, F. Chen, D. Wang, Y. Zhang, D. Han, T. Wang, G. Gu, *Soft Rob.* **2020**, *7*, 583.
[35] C. Fu, Z. Xia, C. Hurren, A. Nilghaz, X. Wang, *Biosens. Bioelectron.* **2022**, *196*, 1.
[36] A. Maziz, A. Concas, A. Khaldi, J. Stalhand, M.-K. Persson, E. W. H. Jager, *Sci. Adv.* **2017**, *3*, 1600327.
[37] S. Poincloux, M. Adda-Bedia, F. Lechenault, *Phys. Rev. X* **2018**, *8*, 021075.
[38] F. Sun, X. Hu, *Mater. Res. Express* **2020**, *7*, 075306.
[39] S. Liu, Z. Du, K. Xie, G. Liu, S. Yang, *Fibers Polym.* **2018**, *19*, 2411.
[40] R. Wu, S. Liu, Z. Lin, S. Zhu, L. Ma, Z. L. Wang, *Adv. Energy Mater.* **2022**, *12*, 2201288.
[41] K. E. Grabowska, *Text. Res. J.* **2010**, *80*, 1917.
[42] J. Abel, J. Luntz, D. Brei, *Smart Mater. Struct.* **2013**, *22*, 125001.
[43] L. Lu, G. Jiang, G. Wu, *Text. Res. J.* **2021**, *92*, 479.
[44] F. Sun, R. A. M. Asad, Z. Du, W. Yu, N. Chen, *Fibers Polym.* **2015**, *16*, 1395.
[45] S. Chen, Y. Pang, Y. Cao, X. Tan, C. Cao, *Adv. Mater. Technol.* **2021**, *6*, 2100084.